ISBN(softcover): 978-3-0364-0995-5 ISBN(eBook): 978-3-0364-1995-4

Table of Contents

Preface

Mechanical Evaluation of 6060 Aluminum Alloy under Elevated Extrusion Ram Speed Using Liquid Nitrogen Die Cooling
E. Giarmas, E.K. Tzimtzimis, K. Tsongas and D. Tzetzis 1

An Experimental Investigation of the Effect of Compression Calibration on the Ductility of AA6061 Extrusions
M.C. Uzun and T. Welo 15

Numerical Investigation of Round Profile Production: A Fem-Based Comparison between Friction Stir Extrusion and Conventional Extrusion
C. Acerbi, M. Negozio, A.H.A. Lutey, M. Felci, U.F.H. Suhuddin, H.S. Rana, B. Klusemann and S. Bocchi 25

Compensating Property Fluctuations in Cold Extrusion Using Adaptive Dies
C. Siedbürger and P. Groche 35

Lightweight Battery Housings from Thin-Walled, Large-Scale Aluminum Profiles by Hot Extrusion
O. Schulz, S. Wurth, A. Selvaggio, J. Gebhard, Y.P. Korkolis, P. Bieker and T. Kloppenborg 51

Calibrating a Lode-Parameter-Dependent Damage Evolution Equation to Cold Extrusion Experiments
R. Gitschel, A.E. Tekkaya and Y.P. Korkolis 63

Effect of Chemical Composition on Hot Extrudability and Tribological Behavior of 7000 Series Aluminum Alloys
S. Ngernbamrung, K. Dohda, T. Funazuka, J. Oshima and T. Shiratori 73

Using Tungsten Inert Gas Welding Equipment to Locally Heat Tubes and Achieve Inhomogeneous Thickness in Tube Sinking Processes
L.I. Besong and J. Buhl 83

Charge Weld Evolution in Profile Extrusion: Variability across Billets and Multi-Profile Designs
I. Kniazkin, I. Kulakov and N. Biba 93

Development of a System for Ultrasonic Die Oscillations during Extrusion of Aluminum Hollow Profiles
T. Thomas, M. Negendank, N. Laengst, V. Merklinger, J. Maier and S. Mueller 109

Detection of Charge Welds in Lateral Angular Co-Extrusion Using Non-Destructive Testing
A. Verschinin, F.P. Schäfke, N. Mohnfeld, H.J. Maier, J. Uhe, C. Klose and S. Barton 121

Comparative Characterization through Torsion Tests of Primary and Secondary Aluminum Alloys for the Extrusion Process
N. Lai, S. Di Donato, L. Donati, R. Pelaccia, B. Reggiani and M. Negozio 133

Transient Thermal Analysis of Multiple Extrusion Runs with Nitrogen Cooling by Means of Qform Code
R. Pelaccia, S. Di Donato, M. Negozio, N. Lai, B. Reggiani and L. Donati 151

Numerical Data-Driven Modelling of Modified Samanta Process for Cold Extrusion of Gears
T. Deliktas, M. Görz, A. Schenek, M. Speth and M. Liewald 165

Key Engineering Materials
ISSN: 1662-9795, Vol. 1048, pp 25-34
doi:10.4028/p-hyK7OT

Submitted: 2025-12-17
Revised: 2026-02-16
Accepted: 2026-02-23
Online: 2026-04-14

Numerical Investigation of Round Profile Production: A FEM-Based Comparison between Friction Stir Extrusion and Conventional Extrusion

ACERBI Carlo[1,a*], NEGOZIO Marco[1,b], LUTEY Adrian H.A.[1,c], FELCI Matteo[1,d], SUHUDDIN Uceu F.H.[2,e], RANA Harikrishna[2,f], KLUSEMANN Benjamin[2,3,g] and BOCCHI Sara[4,h]

[1]University of Parma, Department of Engineering for Industrial Systems and Technologies DISTI, Parco Area delle Scienze, 181/A, 43124 Parma, Italy

[2]Helmholtz-Zentrum Hereon, Institute of Material and Process Design, Solid State Material Processing, Max-Planck-Straße 1, 21502 Geesthacht, Germany

[3]Leuphana University Lüneburg, Institute for Production Technology and Systems, Universitätsallee 1, 21335 Lüneburg, Germany

[4]University of Bergamo, Department of Management, Information and Production Engineering, Via Pasubio 7/b, 24044 Dalmine, BG, Italy

[a]carlo.acerbi@unipr.it, [b]marco.negozio@unipr.it, [c]adrianhughalexander.lutey@unipr.it, [d]matteo.felci@studenti.unipr.it, [e]uceu.suhuddin@hereon.de, [f]harikrishnasinh.rana@hereon.de, [g]benjamin.klusemann@hereon.de, [h]sara.bocchi@unibg.it

Keywords: Process sustainability; Friction Stir Extrusion; Finite Element Analysis; Process optimization.

Abstract. Friction Stir Extrusion, Direct Extrusion and Indirect Extrusion are all valid processes for the production of round extrudates. However, differences and similarities between them have yet to be analyzed by the scientific community, since with the same geometry, each technology instills specific properties to the extruded product. In this context, the present work presents an in-depth analysis via QForm UK Finite Element Method software of the effect that each process has on a AA6061 extruded wire. Various combinations of rotational speed (200, 400, 600 rpm), feed rate (1, 2, 3, 4 mm/s) and pre-heating temperature (450, 500°C) were analyzed to assess differences and similarities between the different processes.

Introduction

In the production of extrudates, numerous technologies can be employed, from conventional Direct Extrusion (DE) and Indirect Extrusion (IE), to the novel Friction Stir Extrusion (FSE) process. Developed by The Welding Institute (Cambridge, UK) in 1993, FSE is gaining increasing attention for its solid-state recycling capabilities and high energy efficiency [1]. This technology employs a rotating tool in combination with a die. The frictional heat generated during processing softens the workpiece material, which is subsequently forced through the die to form an extruded profile [2]. The primary process parameters in FSE are the rotational speed and the feed rate, together with the tool geometry [2,3]. The intense thermomechanical conditions experienced during the process promote significant microstructural evolution, which may result in enhanced overall mechanical properties [4]. Another distinctive feature of FSE is its ability to produce extruded components not only from solid billets but also from alternative feedstock materials such as chips or powders [5]. The macroscopical mechanical properties of a material derive from its microstructure, which is affected by a variety of factors. For instance, hardness, yield strength and ultimate tensile strength are correlated with grain size, dislocation density and element distribution within the alloy [6]. Especially in high-temperature processes such as FSE, predicting microstructure evolution is a complex task. Thus, an in-depth study of the physical characteristics of each process is fundamental to obtain the desired mechanical properties for a given application.

Among aluminum alloys, those of the 6xxx group (Al-Mg-Si alloys) compose the majority of extruded components, due to their high formability and low cost [7,8]. AA6061 (AlMg1SiCu) is one of the most widely known alloys, for its ability to be age-hardened thanks to the precipitation of the β-Mg_2Si phase from a supersaturated solid solution [9,10]. Thus, AA6061 was chosen as the subject material for this study.

DE and IE have been subjected to a wide number of studies, both experimental and numerical, devoted to process optimization, in terms of waste, microstructure, die cooling, properties of the extruded profile, and defects. For instance, Pelaccia et al. [11] have researched the potential of liquid nitrogen cooling in the extrusion of AA6063 and ZM21 alloys, through experimental and numerical analyses, obtaining excellent results and a valid numerical model able to predict the experimental outcome with temperature errors below 8% and load errors below 11%. In another study, Kniazkin at al. [12] analyzed the billet skin defect with the software QForm UK, validating the predictive model via experimental studies. They showed a good numerical-experimental match, and reduced simulation time with respect to prior studies. Negozio et al. [13] introduced a novel AA6063 recrystallization model, performing calibration and validation via experimental analysis and numerical FEM simulations using the software QForm UK. The authors accurately modelled the static and dynamic recrystallization behavior, with prediction errors remaining always below ± 25%. In another study, Negozio et al. [14] predicted grain size and Peripheral Coarse Grain defect formation, combining empirical microstructural observations and data from FEM simulations to train an Artificial Neural Network (ANN), demonstrating increased prediction accuracy compared to state-of-the-art analytical models, and potential for tailoring process parameters to achieve desired microstructure in an actual manufacturing environment.

On the other hand, not much research has been devoted to the understanding and optimization of the FSE process, demonstrating the need for further analysis. Bocchi et al. [15] investigated the recrystallization mechanism and bonding phenomenon within the FEM software DEFORM 3D, applying a recrystallization model originally developed for conventional extrusion. They found their models to accurately predict process kinetics, including bonding and microstructure evolution. Negozio et al. [16] developed a robust model for predicting bonding phenomena and recrystallization occurring during the FSE of AA6061 powder. Validation was based on an experimental campaign in which AA6061 powder was FSEed at different rotational speeds and feed rates. In another study, Li et al. [17] reported the effect of process parameters such as extrusion force and feed rate on deformation behavior of aluminum alloys during FSE. Material flow patterns were obtained and correlated with extrusion temperature, emphasizing the importance of strain for both bonding condition and process optimization. In a similar work, Li et al. [18] analyzed material flow in AA6061 alloy thanks to the introduction of a AA2195 marker, showing that deformation behavior is highly affected by extrusion force and feed rate. Zhang et al. [19] performed heat transfer and temperature field analyses during the FSE of AA6061, developing a numerical model that correctly predicts temperature variations within the workpiece. Diyoke et al. [20] have performed a finite element analysis (FEA) on FSE and conventional extrusion, to assess the effect that friction condition has on shear, material flow and the consequent thermo-mechanical condition. The numerical results showed a reduction in extrusion force in FSE compared to conventional extrusion, together with homogeneous grain refinement in the case of sticking friction condition. However, to the authors' best knowledge, no further research has focused on the numerical comparison between FSE and conventional extrusion for the AA6061 alloy.

In this context, the present paper presents an in-depth numerical analysis of FSE, DE and IE within the software QForm UK, in terms of extrusion temperature, strain and strain rate evolution during the extrusion of a round AA6061 workpiece. By varying rotational speed, feed rate and DE/IE billet pre-heating temperature, several conditions have been studied to provide a sufficiently large dataset.

Procedure

The Computer Aided Design (CAD) model is displayed in Fig. 1. This model was already proposed by Negozio et al. [16]. The FEA was carried out using the software QForm UK, in order to simulate

FSE, DE and IE processes. The FSE simulations were conducted by varying the rotational speed of the container (200, 400 and 600 rpm) and the die feed rate (1, 2, 3 and 4 mm/s), as summarized in Table 1. No pre-heating temperature was imposed, since in FSE the material heating is related to the frictional and plastic dissipation rather than from external thermal input [2]. The DE and IE simulations were performed using the same feed rates adopted for the FSE cases. The main distinction for DE lies in the definition of tool kinematics, as in direct extrusion the material flow is driven by the ram motion, which directly imposes the extrusion speed. Both the DE and IE presented no rotational speed and billet pre-heating temperatures of 450 and 500 °C (Table 2).

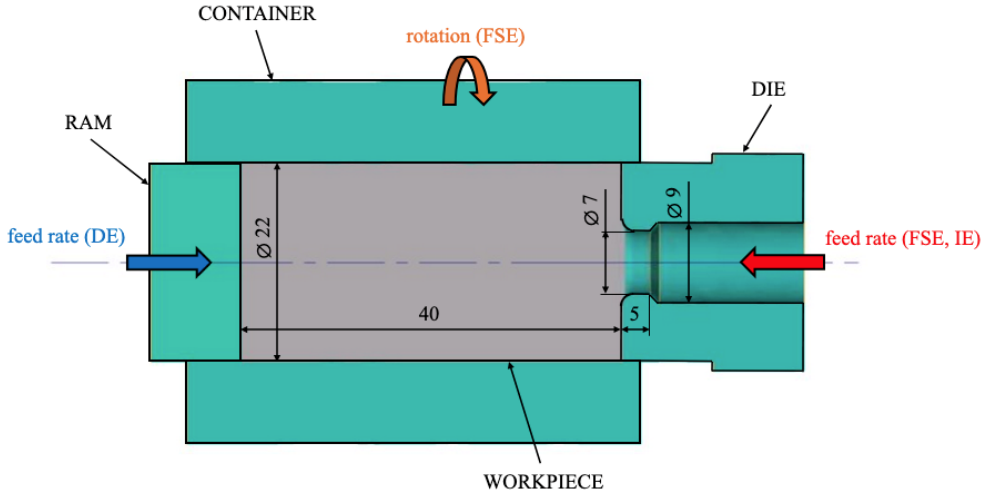

Fig. 1. CAD model used for the simulations, with the main process parameters and dimensions displayed.

Table 1. Process parameters used for FSE simulations.

Parameter	Value
Rotational speed [rpm]	200, 400, 600
Feed rate [mm/s]	1, 2, 3, 4
Feedstock temperature	20°C (room temperature)

Table 2. Process parameters used for DE and IE simuations.

Parameter	Value
Extrusion mode	direct, indirect
Feed rate [mm/s]	1, 2, 3, 4
Pre-heating temperature [°C]	450, 500

The AA6061 material properties were calculated according to the Qform UK database. These properties were determined through linear interpolation of the AA6061 parameters at 20 °C and 500 °C, as reported in Table 3. The die and the container have been considered as rigid bodies made of AISI H13 steel, whose properties have also been taken from the software library.

Table 3. Properties of AA6061 at 20 and 500°C, used for linear interpolation.

Property	Value at 20°C	Value at 500°C
Density [kg/m^3]	2705	2592
Thermal conductivity [W/(m·K)]	185	237
Thermal expansion [1/°C]	2.21 E-5	2.80 E-5
Specific heat [J/(kg·K)]	898	1020
Young's modulus [MPa]	72000	46000
Poisson's coefficient	0.33	0.36

The flow stress (σ_f) was calculated using the Hensel-Spittel equation (Eq. 1).

$$\sigma_f = A \cdot e^{m_1 \cdot T} \cdot \varepsilon^{-m_2} \cdot \dot{\varepsilon}^{-m_3} \cdot e^{m_4/\varepsilon} \cdot (1+\varepsilon)^{m_5 \cdot T} \cdot e^{m_7 \cdot \varepsilon} \cdot \dot{\varepsilon}^{m_8 \cdot T} \cdot T^{m_9}, \quad (1)$$

where ε is the true strain, $\dot{\varepsilon}$ the true strain rate, and T the absolute temperature. The coefficients A, m_1–m_9 are material constants, whose values have been taken from [16] (Table 4).

Table 4. Coefficients used in the Hensel-Spittel equation. [16]

Coefficient	Value
A [MPa]	5179.35
m_1 [K^{-1}]	-0.0065
m_2	0.0054
m_3	-0.2285
m_4	-0.0002
m_5 [K^{-1}]	0.0014
m_7	-0.6683
m_8 [K^{-1}]	-0.0005
m_9	0

In the FSE model, friction between tools and workpiece was modeled according to Levanov's formulation (Eq. 2), in which the tangential stress (τ) is calculated as a combination of Coulomb's and Siebel's models:

$$\tau = m \cdot \frac{\sigma_f}{\sqrt{3}} \cdot \left(1 - e^{-n \cdot \sigma_n / \sigma_f}\right), \quad (2)$$

where σ_f is the flow stress, σ_n is the normal stress, and m, n are the friction and Levanov's coefficients, respectively, for FSE (Table 5). In DE and IE, the friction parameters were taken from [14], where a sticking condition is assumed between the workpiece and the die, the ram and the container, and Levanov's model is applied for the profile interaction with the bearing section ($m = 0.3$, $n = 1.25$). The thermal parameters were taken from [21], and are reported in Table 6.

Table 5. Coefficients for Levanov's friction model.

Coefficient	Value
m	0.6
n	1.25

Table 6. Thermal parameters of the AA6061 workpiece [21].

Coefficient	Value
Tool-workpiece heat exchange coefficient [W/(m^2·K)]	11,000
Air temperature [°C]	20
Workpiece emissivity	0.25
Air-workpiece heat exchange coefficient [W/(m^2·K)]	20

The model for FSE has been validated in [16] by comparing experimental and numerical extrusion loads, with errors below 5%. On the other hand, the conventional extrusion model has been validated in other published papers [14].

The FEM output variables considered in the study are temperature, strain and strain rate, measured at 50% of the die/ram stroke. Both temperature and strain were calculated using the default software algorithms, while a specifically designed subroutine was introduced for strain rate, whose purpose was to store the maximum strain rate experienced by each point during the simulation.

Due to the high thermal conductivity of aluminum alloys, only one temperature value was taken as representative for a specific cross-section. However, for strain and maximum strain rate, six measurements were made along the radius of the extruded wire, in order to create a profile of the given property (Fig. 2). For simplicity, strain and strain rate profiles were plotted against a normalized position, for which 0 equals to the core of the wire and 1 to its surface.

The obtained results have then been confronted with those from the other simulations, in order to evaluate differences and similarities between FSE, DE and IE processes.

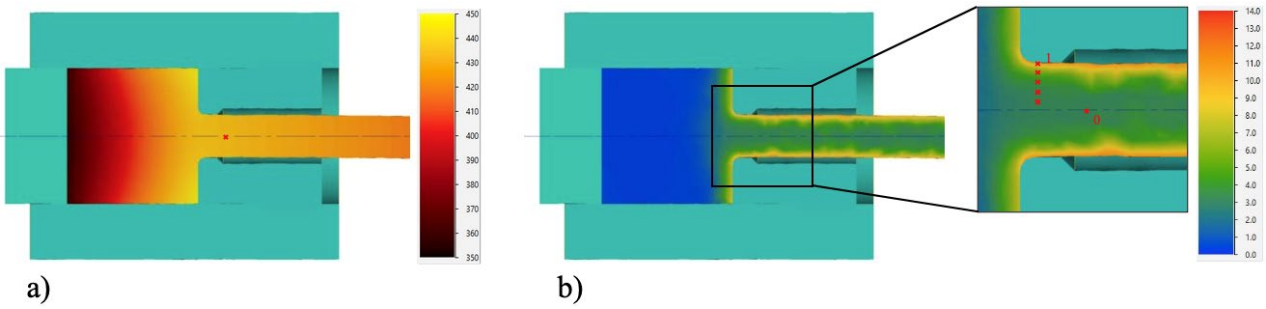

Fig. 2. Simulation results in terms of a) temperature, and b) strain, together with probed points, for FSE at 400 rpm and 2 mm/s.

Results and Discussion

In this section, the outcomes of the numerical analysis are presented, performing an in-depth comparison between FSE and conventional DE and IE.

Temperature. Temperature results for FSE, DE and IE are presented in Table 7 and Table 8. The first notable difference between the processes is that increasing the feed rate leads to opposite effects on the extrusion temperature (Fig. 3). In the FSE process, a higher feed rate reduces the peak temperature because the shorter interaction time limits heat generation. Conversely, in DE and IE, increasing the feed rate raises the extrusion temperature, as more energy is required for deformation and higher frictional heating is generated. DE shows slightly higher temperatures than IE, due to the well-known differences in process characteristics, but pre-heating temperature seems to be the main factor influencing extrusion temperature. An increase in rotational speed leads to higher temperatures as a result of enhanced frictional heating, enabling the FSE process to operate over a wider range of profile exit temperatures compared to conventional DE and IE processes.

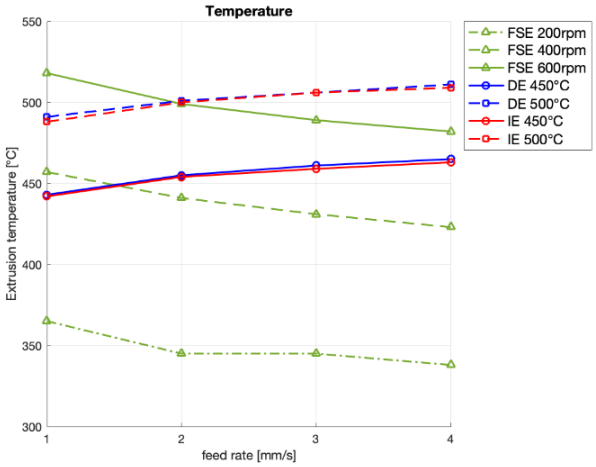

Fig. 3. Extrusion temperature results for FSE, DE and IE.

Table 7. Simulation results in terms of extrusion temperature for FSE.

Feed rate [mm/s]	Rotational speed [rpm]	Extrusion temperature [°C]
1	200	365
2	200	345
3	200	345
4	200	338
1	400	457
2	400	441
3	400	431
4	400	423
1	600	518
2	600	499
3	600	489
4	600	482

Table 8. Simulation results in terms of extrusion temperature for DE and IE.

Feed rate [mm/s]	Pre-heating temperature [°C]	Extrusion temperature [°C]	
		direct	indirect
1	450	443	442
2	450	455	454
3	450	461	459
4	450	465	463
1	500	491	488
2	500	501	500
3	500	506	506
4	500	511	509

Strain. Strain results for FSE, DE and IE for core and surface are presented in Table 9 and Table 10. Each investigated extrusion technology, although still influenced by die design, affects strain through distinct mechanisms governed by the process kinetics and the specific parameters (Fig. 4). Similarly to the temperature results, an increase in feed rate leads to a decrease in surface strain for FSE. However, this increase does not significantly affect the maximum strain results in DE and IE (Fig. 4). Indeed, a higher feed rate in FSE causes a decrease in the material deformation path that leads to lower value of surface strain. In the core area, strain values are similar, with FSE showing slightly higher values. Indeed, at the center, almost no rotation is experienced during both FSE and conventional extrusion, causing the similarities in strain values for normalized position close to 0 shown in Fig. 4.

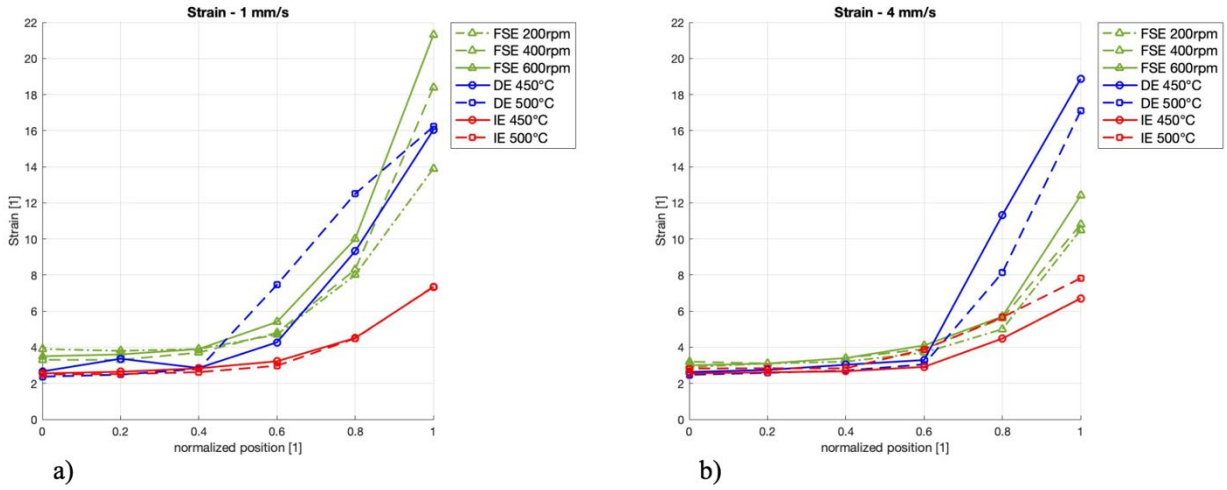

Fig. 4. Strain results for FSE, DE and IE, at a) 1 mm/s, and b) 4 mm/s, plotted against a normalized position ("0" = core, "1" = surface).

Table 9. Simulation results in terms of strain at surface and core for FSE.

Feed rate [mm/s]	Rotational speed [rpm]	Surface strain [1]	Core strain [1]
1	200	13.9	3.9
2	200	10.6	3.0
3	200	10.2	3.0
4	200	10.5	2.9
1	400	18.4	3.3
2	400	13.8	3.2
3	400	11.3	3.0
4	400	10.8	3.2
1	600	21.3	3.5
2	600	16.0	3.2
3	600	14.3	3.1
4	600	12.4	3.0

Table 10. Simulation results in terms of strain at surface and core for DE and IE

Feed rate [mm/s]	Pre-heating temperature [°C]	Surface strain [1]		Core strain [1]	
		direct	indirect	direct	indirect
1	450	16.0	7.3	2.7	2.6
2	450	16.0	6.8	2.4	2.7
3	450	16.7	7.7	2.5	2.5
4	450	18.9	6.7	2.6	2.6
1	500	16.2	7.4	2.4	2.5
2	500	17.2	7.2	2.6	2.7
3	500	20.6	7.5	3.2	2.5
4	500	17.1	7.8	2.5	2.8

Strain rate. Strain rate results for FSE, DE and IE at core and surface are presented in Table 11 and Table 12. These processes show some similarities in strain rate trends (Fig. 5). In all cases, an increase in feed rate leads to an increase in surface strain rate values, due to a required shorter time for the deformation process. In FSE, when the feed rate increases from 1 to 4 mm/s, there is a moderate rise in maximum strain rate. However, these values remain high, reaching 45.5 s^{-1} at 1 mm/s and 600 rpm, and 52.0 s^{-1} at 4 mm/s and 600 rpm. For DE and IE, on the other hand, feed rate has a more pronounced effect on the surface strain rate. As visible in Fig. 5, with a pre-heating temperature of 500 °C, DE

and IE show an increase in strain rate from 7.8 and 6.3 s^{-1} at 1mm/s to 35.0 and 26.5 s^{-1} at 4 mm/s, respectively. In addition, increasing rotational speed in FSE increases surface strain rate, due to the higher velocity of material flow. Again, core values are similar between the two processes, but in this case FSE tends to exhibit slightly lower strain rates.

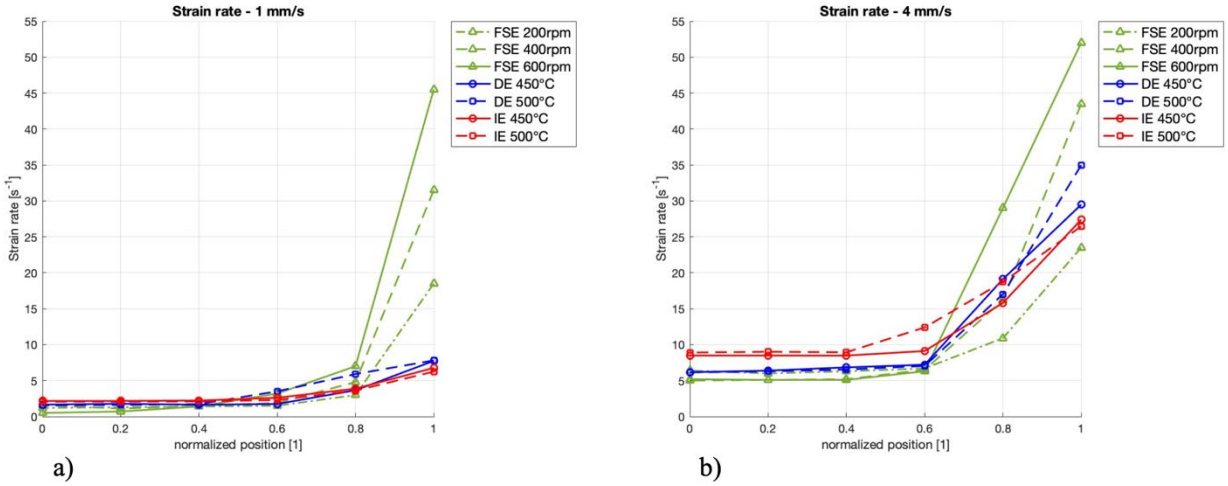

Fig. 5. Strain rate results for FSE, DE and IE, at a) 1 mm/s, and b) 4 mm/s, plotted against a normalized position ("0" = core, "1" = surface).

Table 11. Simulation results in terms of strain rate at surface and core for FSE.

Feed rate [mm/s]	Rotational speed [rpm]	Surface strain rate [s^{-1}]	Core strain rate [s^{-1}]
1	200	18.5	1.2
2	200	19.0	3.3
3	200	20.5	4.7
4	200	23.5	6.4
1	400	31.5	1.6
2	400	35.5	2.2
3	400	42.5	3.9
4	400	43.5	5.0
1	600	45.5	0.5
2	600	47.0	2.8
3	600	49.0	4.2
4	600	52.0	5.2

Table 12. Simulation results in terms of strain rate at surface and core for DE and IE.

Feed rate [mm/s]	Pre-heating temperature [°C]	Surface strain rate [s^{-1}]		Core strain rate [s^{-1}]	
		direct	indirect	direct	indirect
1	450	7.7	6.8	1.7	2.2
2	450	12.0	13.7	3.0	4.3
3	450	20.8	20.7	4.8	6.4
4	450	29.5	27.4	6.2	8.5
1	500	7.8	6.3	1.6	2.1
2	500	13.9	12.6	3.1	4.3
3	500	22.2	21.8	4.8	6.2
4	500	35.0	26.5	6.2	8.9

Summary

The present work involved an in-depth numerical analysis using the FEM software QForm UK, in order to assess differences and similarities between the FSE and the conventional DE and IE processes.
The main outcomes of this paper are:

1. Increasing the feed rate leads to a decrease in extrusion temperature for FSE, while it increases for DE and IE.
2. All processes show similar strain profiles, but upon an increase in feed rate, the surface strain for FSE decreases, while it increases for DE and IE. This causes FSE to present higher surface strain values at low feed rates, and lower surface strain than DE at higher feed rates.
3. All processes show similar strain rate trends, and an increase in feed rate leads to an increase in surface strain rate for all processes. FSE shows high values of maximum strain rate in all conditions, though lower than DE and IE at low rotational speeds and high feed rates.

Conclusively, FSE shows higher extrusion temperature, higher surface strain and tendentially higher surface strain rates than DE and IE at low feed rates and high rotational speeds. In this condition, FSE can produce a finer microstructure thanks to the elevated strain values. This does not directly translate in better mechanical properties, due to the variety of factors involved. However, alloys that do not tend to recrystallize like 6082 aluminum alloy [22] could benefit from FSE, allowing the production of high-quality round profiles. The trend is inverted at high feed rates and low rotational speeds. Core values of strain and strain rate are similar between all processes.

References

[1] V. (Kiran) Manchiraju, Direct Solid-State Conversion of Recyclable Metals and Alloys, 2012.

[2] M. Akbari, P. Asadi, R.A. Behnagh, F. Bedir, N. Choupani, T. Sadowski, Process Parameters and Tool Design in Friction Stir Extrusion: A Sustainable Recycling Technique, Engineering Reports 7 (2025).

[3] D. Baffari, G. Buffa, L. Fratini, A numerical model for Wire integrity prediction in Friction Stir Extrusion of magnesium alloys, J. Mater. Process. Technol. 247 (2017) 1–10.

[4] G. Ingarao, D. Baffari, E. Bracquene, L. Fratini, J. Duflou, Energy Demand Reduction Of Aluminum Alloys Recycling Through Friction Stir Extrusion Processes Implementation, Procedia Manuf. 33 (2019) 632–638.

[5] L. Rath, U.F.H. Suhuddin, B. Klusemann, Comparison of Friction Extrusion Processing From Bulk and Chips of Aluminum-Copper Alloys, Key Eng. Mater. 926 (2022) 471–480.

[6] E. Cerri, E. Ghio, Aging Profiles of AlSi7Mg0.6 and AlSi10Mg0.3 Alloys Manufactured via Laser-Powder Bed Fusion: Direct Aging versus T6, Materials 15 (2022) 6126.

[7] M. Cai, G.J. Cheng, Microstructure-properties relationship in two Al-Mg-Si alloys through a combination of extrusion and aging, JOM 59 (2007) 58–61.

[8] S.J. Murtha, New 6XXX Aluminum Alloy for Automotive Body Sheet Applications, in: 1995.

[9] J. Buha, R.N. Lumley, A.G. Crosky, Microstructural development and mechanical properties of interrupted aged Al-Mg-Si-Cu alloy, Metallurgical and Materials Transactions A 37 (2006) 3119–3130.

[10] G.A. Edwards, K. Stiller, G.L. Dunlop, M.J. Couper, The precipitation sequence in Al–Mg–Si alloys, Acta Mater. 46 (1998) 3893–3904.

[11] R. Pelaccia, M. Negozio, L. Donati, B. Reggiani, L. Tomesani, Extrusion of Light and Ultralight Alloys with Liquid Nitrogen Conformal Cooled Dies: Process Analysis and Simulation, J. Mater. Eng. Perform. 31 (2022) 1991–2001.

[12] I. Kniazkin, R. Pelaccia, M. Negozio, S. Di Donato, L. Donati, B. Reggiani, N. Biba, Rezvykh Ruslan, I. Kulakov, Investigation of the skin contamination predictability by means of QForm UK extrusion code, in: 2023: pp. 543–552.

[13] M. Negozio, A. Segatori, R. Pelaccia, B. Reggiani, S. Di Donato, L. Donati, Modeling of recrystallization behaviour of AA6xxx aluminum alloy during extrusion process, Transactions of Nonferrous Metals Society of China 34 (2024) 3170–3184.

[14] M. Negozio, L. Donati, A.H.A. Lutey, Smart extrusion via data-driven prediction of grain size and peripheral coarse grain defect formation, Sci. Rep. 15 (2025) 9518.

[15] S. Bocchi, M. Negozio, C. Giardini, L. Donati, Prediction of the microstructure evolution during the friction stir extrusion of a AA6061 aluminum alloy, in: 2024: pp. 678–687.

[16] M. Negozio, S. Bocchi, L. Rath, E. Ghio, Finite element modeling of microstructure evolution and bonding during Friction Stir Extrusion of AA6061 powder at different tool feed rates and rotational speeds, Mater. Charact. 219 (2025) 114639.

[17] X. Li, W. Tang, A.P. Reynolds, W.A. Tayon, C.A. Brice, Strain and texture in friction extrusion of aluminum wire, J. Mater. Process. Technol. 229 (2016) 191–198.

[18] X. Li, W. Tang, A.P. Reynolds, Material Flow and Texture in Friction Extruded Wire, in: Friction Stir Welding and Processing VII, Springer International Publishing, Cham, 2013: pp. 339–347.

[19] H. Zhang, X. Li, W. Tang, X. Deng, A.P. Reynolds, M.A. Sutton, Heat transfer modeling of the friction extrusion process, J. Mater. Process. Technol. 221 (2015) 21–30.

[20] G. Diyoke, L. Rath, R. Chafle, N. Ben Khalifa, B. Klusemann, Numerical simulation of friction extrusion: process characteristics and material deformation due to friction, International Journal of Material Forming 17 (2024) 26.

[21] S. Bocchi, G.D. D'Urso, C. Giardini, G. Maccarini, A Simulative Method for Studying the Bonding Condition of Friction Stir Extrusion, Key Eng. Mater. 926 (2022) 2333–2341.

[22] C. Poletti, R. Bureau, P. Loidolt, P. Simon, S. Mitsche, M. Spuller, Microstructure Evolution in a 6082 Aluminium Alloy during Thermomechanical Treatment, Materials 11 (2018) 1319.